Functional Fits to Some Observed Drop Size Distributions and Parameterization of Rain

PAUL T. WILLIS

Atlantic Oceanographic and Meteorological Laboratory, Hurricane Research Division, NOAA, Miami, FL 33149

(Manuscript received 19 May 1983, in final form 3 February 1984)

ABSTRACT

A data sample of optical spectrometer measurements that were obtained in two tropical cyclones is analyzed. The resultant drop size distributions are normalized and their shape is found to exhibit some curvature—departure from exponentiality. When the sample, ordered by rainfall rate, is divided in half, the shape (curvature) of the low-rainfall-rate half is found to be nearly identical to that of the high-rainfall-rate half.

Five functional fits to the data are explored in detail; three are exponential fits—Marshall-Palmer, least-squares and "analytical"—and two are gamma distribution function fits—an analytical and a curvilinear least-squares. The goodness-of-fit is evaluated based on error squared, and on coalescence growth error and drop evaporation error. The coalescence growth and drop evaporation are computed using simple microphysical models. The fits that are based on minimizing squared error do not characterize coalescence growth and evaporation well. An analytical gamma distribution function fit to the measured distributions provided the most reasonable compromise between satisfactory squared-error fit and realistic characterization of coalescence growth and drop evaporation.

With this analytical gamma distribution function fit in mind, modifications to the widely used Marshall-Palmer-based microphysics parameterizations are proposed. These proposed simple modifications should provide a more realistic characterization of coalescence growth and drop evaporation in numerical simulations.

Relations between several bulk parameters of the measured distributions and several parameters of the functional fits are derived. These relations are compared with those found by other investigators.

1. Introduction

Raindrop size distributions are the end product of all of the cloud microphysical processes, cloud dynamical processes and interactions that affect the formation and growth of liquid precipitation. In addition, the raindrop distributions, once formed, can interact with the essential dynamics of the clouds through water loading, precipitation unloading, downdraft initiation by precipitation drag and downdraft maintenance through precipitation evaporation. Warm rain processes in warm-base convective clouds, obviously important in the tropics, also play an important role in a significant fraction of midlatitude summer precipitation.

Besides being directly important microphysically, the raindrop size distributions are also important in the parameterizations of cloud microphysical processes used in the numerical simulation of clouds and larger scale systems. Traditionally, microphysical parameterizations have followed Kessler (1969), dividing condensed water into two categories, cloud water and precipitation water. In this parameterization, the precipitation water is assumed to be distributed exponentially with drop diameter, as first suggested by Marshall and Palmer (M–P) (1948):

$$N(D) = N_0 \exp(-\lambda D), \tag{1}$$

where D is drop diameter and $N(D)dD$ is the concentration of drops having diameters between D and $D + dD$. Marshall and Palmer found that the slope parameter λ depends on rainfall rate R and is given by

$$\lambda = 41R^{-0.21}, \tag{2}$$

where λ has units of cm^{-1} and R is in mm h^{-1}. They also found that the intercept parameter N_0 is a constant $N_0 = 0.08$ cm^{-4}. Nearly all microphysical parameterizations in widespread use distribute precipitation water based on this exponential distribution (1).

If N_0 is assumed to be a known constant, the total precipitation water content M_∞ uniquely determines λ and, thus, the drop size distribution. Here the subscript ∞ on M means that the integrations have been performed up to $D = \infty$. Integrating over the distribution to find the total precipitation water content M_∞ and then solving this expression for λ gives

$$\lambda = \left(\frac{\pi \rho_w N_0^{1/4}}{M_\infty}\right), \tag{3}$$

where ρ_w is the density of the liquid drop. Most prognostic microphysical parameterizations in use assume that N_0 is a constant and use (1) and (3) to distribute the total precipitation water content.

Although the results of theoretical treatments of the evolution of drop distributions generally have been

interpreted as supporting the exponential distribution, the results are not sufficiently definitive to exclude deviation from the exponential. Srivastava (1971) modeled the evolution of the warm rain spectra considering stochastic coalescence and spontaneous drop breakup. Not surprisingly, these results, which did not include collision breakup, showed a large deviation from the M–P distribution, exhibiting a much lower concentration of small drops and a much higher concentration of large drops. Young (1975) and List and Gillespie (1976) conclude that the M–P semilog linearity (exponentiality) is conserved during the evolution of the drop size distributions in rather comprehensive numerical simulations. But, upon close examination, some nonlinearity (curvature) is present in their resultant drop size distributions. List and Gillespie's (1976) collision breakup model produced practically no drops with $D > 2.5$ mm, even though it started with an M–P distribution containing larger drops. Srivastava (1978) assumed an exponential form and solved for evolving N_0 and Λ. For distributions of water content > 1 g m^{-3}, he found that binary interaction processes control the distribution and produce distributions with a nearly constant Λ. Carbone and Nelson (1978), for a rainfall rate of 27.5 mm h^{-1}, find that their theoretical formulation produces an exponential form and that the inclusion of collision breakup makes very little difference in the distribution. Brown (1981) has shown, from a solution of the drop breakup equation, that breakup tends to deplete drops in the larger size categories. Under some conditions, breakup increases the number of drops in sizes near $D = 1.5$ mm, resulting in curvature. However, in this work the interactions involving both coalescence and breakup were not included in the same simulation. Even though theoretical studies generally tend to support the exponential form, it is clear that deviations are possible within this framework.

Measurements from many geographic regions and rain types have shown that the exponential distribution tends to be the limiting form when individually observed drop size distributions are averaged (Rogers, 1979). But, numerous deviations from a strictly exponential distribution have been found, particularly for convective rain situations that involve a significant depth of warm cloud. Joss and Gori (1978), when conventionally averaging many 1 min distributions, found an exponential shape. However, when they averaged the shapes of the same individual 1 min samples, they found that the resultant average shape deviated markedly from the exponential toward monodispersity, i.e., less small and less large drops than either M–P or the best-fit exponential. The shapes were similar to those found in this study, but with a somewhat higher concentration of large drops for the high-rainfall-rate distributions. Takeuchi (1978) fitted a gamma distribution function to observed drop size distributions. Ulbrich (1981) also found that the gamma distribution function closely approximated the resultant drop spectra for observed individual and combined datasets. Mueller and Sims (1966) found that a lognormal distribution fitted a large number of drop size distributions best. Carbone and Nelson (1978), at cloud base in summer convective clouds in Texas, found drop concentrations an order of magnitude lower than did M–P at $D = 1$ mm and concentrations much higher than M–P at $D > 3$ mm, very much at variance with the results of this study. They attribute these large deviations to drop sorting by sedimentation. They accept the extreme spectral forms based on agreement between radar reflectivities calculated from the drop distributions and those measured by radar in the same volume. Even though the M–P exponential fit to observed averaged drop size distributions has attained widespread acceptance and durability, there are numerous indications that it may be possible to improve upon this fit. This is particularly true for short-period samples in convective rain situations.

It is the objective of this study to analyze a dataset of drop size distributions from clouds that have well-developed warm rain processes and that span a wide range of rainfall rates. The shape of the measured drop size distributions is examined using a normalization procedure. Five selected functional fits to the observed data are described. Their performance is evaluated based, not only on the customary squared-error criterion, but also on the goodness of the estimates of drop coalescence growth (accretion) and drop evaporation provided by the fits. Modifications to cloud microphysical parameterizations, using an analytical gamma distribution to distribute the rainwater instead of the exponential distribution, are discussed in some detail. Since the same physical processes that shape the drop distributions are operative in all well-developed warm rain, the results, which are based on data from two tropical cyclones, should be generally applicable to warm-based convective clouds.

2. Method of observation

The imaging optical spectrometer has provided a significant advance in the ability to size precipitation particles. The Particle Measuring Systems (PMS) two-dimensional precipitation optical array spectrometer used in this study not only provides images of undisturbed particles, but provides the additional advantage of digitally recording the images. This allows objective machine data reduction of voluminous quantities of image data. The precipitation probe used in this study measures a diameter range of 100–6500 μm. The data were analyzed from 10 s samples (effectively 10 s minus the overload fraction). Thus, each drop size distribution represents approximately 1.3 km of flight track and a sample volume of 2 m^3. This volume provides an adequate sample for all but the lowest rainfall rates. Although considerable variation in rainfall rate probably

does occur over this path length, this is about the length scale of the convective features involved in the production of the precipitation. This sampling is consistent with the scale of most past observations of drop size distributions. The image data are reduced by a completely objective software routine. Details of the instrument can be found in Knollenberg (1981) and details of the observations and data reduction in Jorgensen and Willis (1982). The dataset analyzed in this study consists of 112 distributions that were measured in Hurricane Anita (3.1 km) and in Hurricane Frederic (0.5 km).

3. Drop size distributions

a. Typical distributions

Four typical drop size distributions from Hurricane Anita are presented in Fig. 1. These distributions are for rainfall rates of 1.85, 15.8, 57.4 and 169.0 mm h^{-1}. The Marshall–Palmer exponential fit is shown in each case. While the M–P fits are fairly good, the spectra appear to be somewhat concave downward, particularly for the high rainfall rates.

b. Determination of spectral shape

It is impractical to present each of the 112 individual drop size distributions used in this analysis. Nevertheless, to allow a determination of the shape of the entire sample, the individual drop size distributions were normalized after the method of Sekhon and Srivastava (SS) (1970). Normalizing the distributions removes the dependence on N_0 and Λ in (1), allowing comparison of the shape of distributions of different rainfall rates.

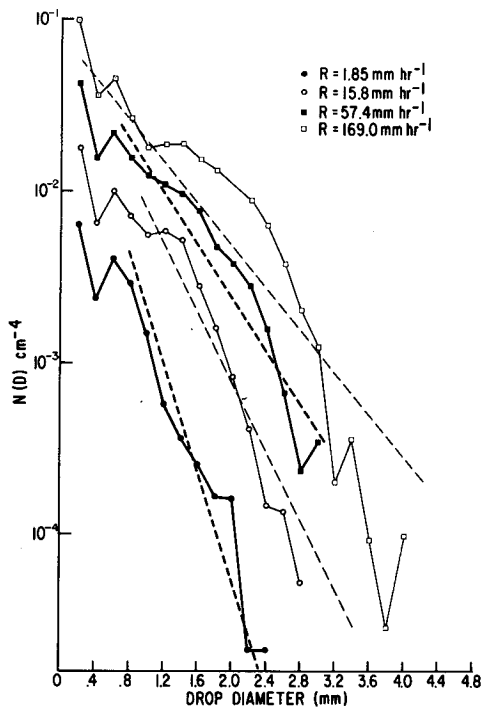

FIG. 1. Four typical drop size distributions and associated Marshall–Palmer fits.

1) NORMALIZATION PROCEDURE

The normalization method involves the elimination of N_0 and λ from (1). First, the precipitation water content M_∞ is found by integrating over all diameters, i.e.,

$$M_\infty = \frac{1}{6}\pi\rho_w \int_0^\infty N_0 D^3 \exp(-\lambda D) dD$$

$$= \frac{\pi\rho_w N_0 \Gamma(4)}{6\lambda^4}, \tag{4}$$

where Γ denotes the gamma function. In actual computation, M_∞ was found by integrating over the range of the instrument. Second, the median volume diameter D_0, dividing the precipitation content of the distribution into two equal parts, is related to the slope of the distribution by

$$D_0 = \frac{\beta}{\lambda}, \tag{5}$$

where β is a constant equal to 3.67, or less, if the distribution is truncated (Atlas, 1953). Eqs. (4) and (5) can now be used to express (1) in nondimensional form as

$$\frac{\rho_w N(D) D_0^4}{M_\infty} = \frac{\beta^4}{\pi} \exp\left(-\beta \frac{D}{D_0}\right). \tag{6}$$

Sekhon and Srivastava (1970, 1971) point out that this normalization provides a "universal" exponential distribution. A semilog plot of $\rho_w N(D) D_0^4 / M_\infty$ versus D/D_0 will yield a straight line of slope $-\beta$ and intercept β^4/π, irrespective of the precipitation rate. Thus, the shapes of numerous drop size distributions can be directly compared on the same plot.

In Fig. 2, the normalized data points from 112 drop size distributions are plotted with $\ln[\rho_w N(D) D_0^4 / M]$ as the ordinate and D/D_0 as the abscissa. The distribution is noticeably concave downward, particularly near $D/D_0 = 1$, indicating some departure from exponentiality. The heavy solid curve was fitted to the data points by means of a curvilinear least-squares routine which is described in Section 3c.

Two exponential curves are also plotted in Fig. 2 for comparison: the M–P curve normalized as above, and the exponential distribution of SS (1971), which was taken from vertical incidence Doppler radar data at 2.1 km elevation in a New England thunderstorm. Qualitatively, the M–P curve captures the essence of the overall distribution of data points. However, the observed concentration of small drops ($D/D_0 < 0.6$)

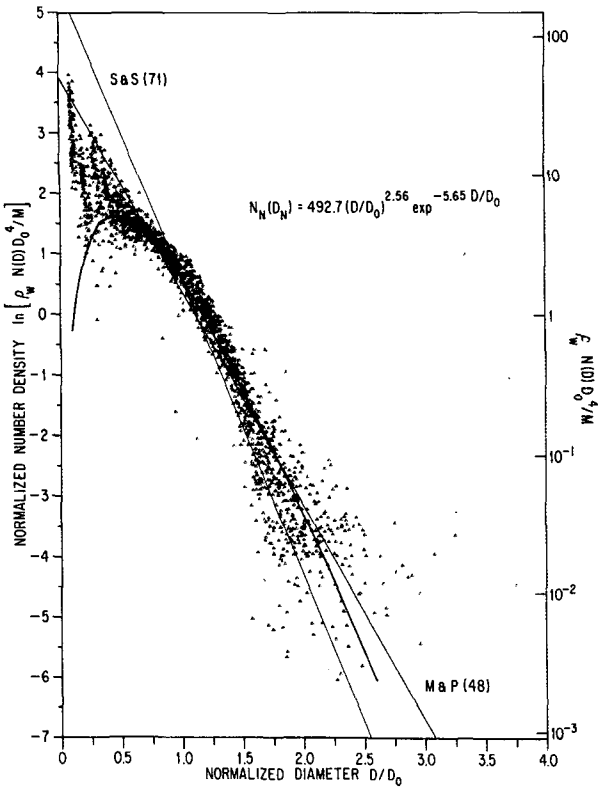

FIG. 2. Sample of 112 drop size distributions normalized after the method of Sekhon and Srivastava (1971). Included for comparison are a gamma distribution function and M–P (1948) and SS (1971) fits.

is considerably less than that indicated by the M–P distribution. At larger sizes ($D/D_0 > 1.5$), observed drop concentrations appear to be slightly less than the M–P distribution. It is significant that SS (1971) also found fewer large drops than indicated by the M–P distribution. This is of significance because their data were obtained from vertical incidence radar scan sample volumes, which should be more than adequate to sample even the largest drops.

Some discussion of the scatter of the data points in Fig. 2 is in order. The points are quite tightly grouped in the middle-sized drop diameters. Part of the scatter at small and large sizes is caused by the distributions not being strictly exponential, as incorrectly assumed in the normalization. In addition, the scatter is caused by sampling and variance in the physical processes shaping the distributions. The increased scatter at the larger sizes is probably due, at least in part, to the minimal sampling volume for large drops. The large scatter at the small diameters ($D/D_0 < 0.6$), which may seem inordinately high at first glance, is really not unexpected. These data were taken largely above cloud base in a wide range of cloud dynamical conditions—updrafts, downdrafts and neutral or inactive, more stratiform, cloud regions. The concentration of the smallest drops is much more sensitive than is the concentration of large drops to the balance between those microphysical processes that produce drops and those that deplete drops. For example, the concentration of small drops can undoubtedly be quite different in an updraft, where small droplets are growing and being replenished by condensation, than in a downdraft where they are being depleted by evaporation. Thus, the high scatter at small drop diameters in Fig. 2 is expected.

To determine whether there were substantial differences in the shape of the distributions between high and low rainfall rates, the sample of drop size distributions, ordered by increasing rainfall rate, was divided roughly in half. The mean rainfall rate of the upper half was 92.4 mm h^{-1} and that of the lower half was 25.1 mm h^{-1}. The two sets of normalized distributions are shown in Fig. 3. There is slightly more scatter in the low rainfall rate set, but the shapes of the two halves are virtually identical. The fits from a curvilinear least-squares gamma function routine to the two halves are nearly identical. The only difference is that the objective fit to the high-rate half indicates a slightly higher normalized number density at low normalized diameters and a slightly lower normalized number density at high normalized diameters, compared with the objective fit to the low-rate half. It is somewhat surprising that the high-rate and low-rate halves of the sample exhibit essentially the same shape characteristics. This similarity indicates that the basic physical processes shaping the spectrum evidently do not change much with rainfall rate over the range represented here.

2) TRUNCATION EFFECTS

The integrations involved in the normalization procedure, as well as in the computation of any higher moments of the distributions, assume that the distributions extend from $D = 0$ to $D = \infty$. At the small size end of the distribution, the probe used in this study measures particles starting at $D = 100$ μm. The practical effects of starting the integrations at $D = 100$ μm, instead of at zero, are negligible. Sekhon and Srivastava (1970) have covered the modifications required for an exponential distribution when the maximum particle diameter is truncated at $D = D_m$, instead of infinity. From the results of SS (1970), which apply to an M–P exponential distribution, if $D_m/D_0 > 2.5$, the distribution may, for practical purposes, be considered to extend to infinity insofar as the values of M and R are concerned. However, the value of Z/Z_∞ for $D_m/D_0 = 2.5$ is 0.8 and for $D_m/D_0 = 3.2$, it is 0.95. For the instrument used in this study the maximum size measured is $D = 6.0$ mm, or larger, because the full particle was not required to be within the diode array. The typical D_0 was between 2.0 and 2.5 mm, even for the highest rainfall rates. As a result, if the distributions are exponential, the effects of truncating

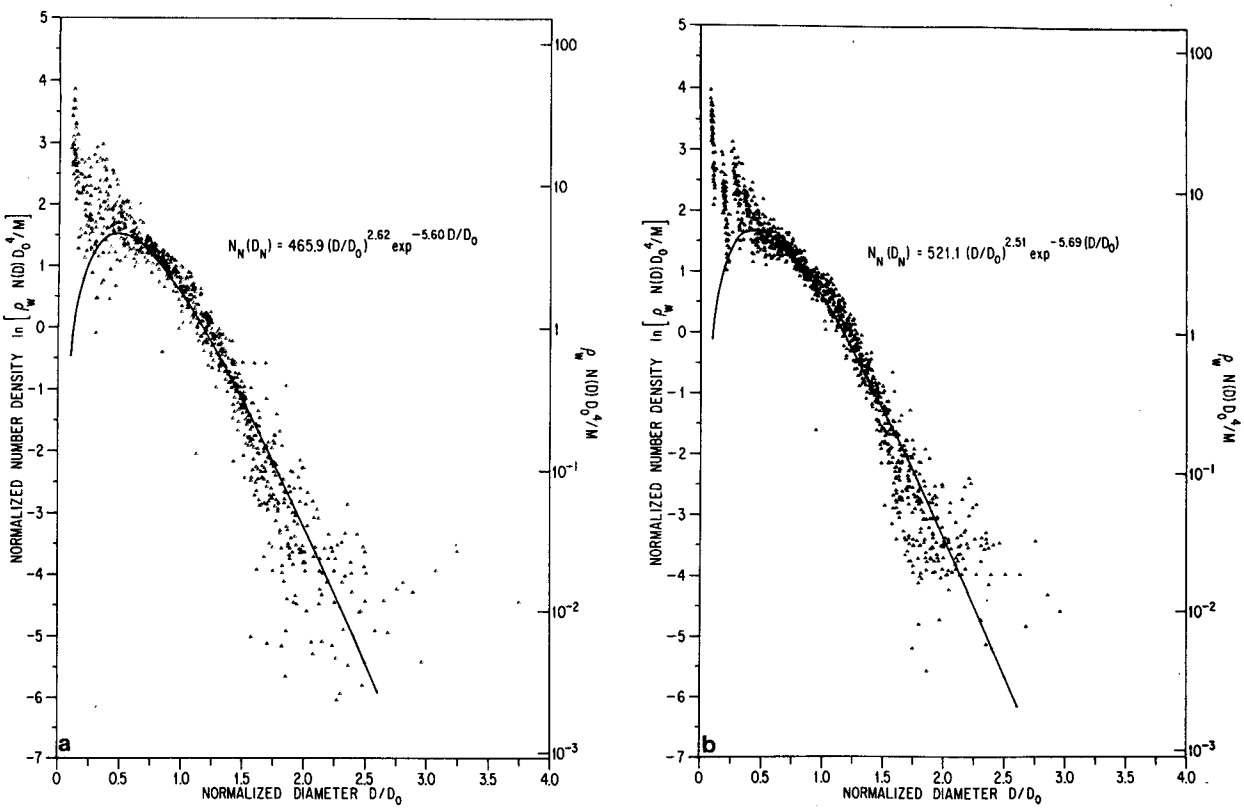

FIG. 3. Drop size distribution sample of Fig. 2 divided into (a) low and (b) high rainfall rate halves and normalized.

the distributions at $D_m = 6$ mm, or slightly larger, are minor based on the analysis of SS (1970).

For a gamma distribution function with a curvature parameter of 2.5, one would intuitively reason that the effects of truncating the distribution at some large diameter would be less than for the exponential distribution. This is true because there are fewer very large drops in this gamma distribution than there are in the M–P exponential of the same water content. The analysis discussed next parallels that of S & S (1970), except that it is for the gamma distribution function.

First, we consider the changes in $\beta(=\Lambda D_0)$ due to truncation at D_m. The median volume diameter is defined as the diameter that divides the total volume of the distribution into two equal parts. For an exponential distribution, the median volume diameter is

$$\int_0^{D_0} D^3 \exp(-\lambda D)dD = \int_0^{D_0} D^3 \exp(-\lambda D)dD. \quad (7)$$

These integrals can be integrated analytically and the resulting equation can be solved numerically to give λD_0 as a function of λD_m, or D_m/D_0. For the gamma distribution with a curvature parameter of $\alpha = 2.5$, the median volume diameter is

$$\int_0^{D_0} D^{5.5} \exp(-\Lambda D)dD = \int_0^{D_0} D^{5.5} \exp(-\Lambda D)dD. \quad (8)$$

Now, because of the non-integer exponents, the integrations must be handled numerically. The result of this numerical integration and numerical solution are shown in Fig. 4a, which gives $\Lambda D_0(\beta)$ as a function of D_m/D_0. It is seen that ΛD_0 reaches its asymptotic value for $D_m = \infty$ of 6.15 when $D_m/D_0 > 2.0$, as compared with a value of about 2.5 for the exponential distribution.

Next we examine the effects of truncation on the integrations required in computing higher moments of the distributions. The appropriate integrals required were evaluated using a table of the incomplete gamma functions. The results of this analysis for W/W_∞ and Z/Z_∞ are compared in Fig. 4b to the curves of SS (1970) for the exponential distribution. Here, F is the ratio of the truncated integration to the integration to $D = \infty$. Even for the sixth moment (Z), if $D_m/D_0 > 2.5$, over 0.95 of the total radar reflectivity factor of the distribution is accounted for in the case of the gamma distribution, while for the exponential only 0.80 is accounted for. Thus, for the gamma distribution and the instrument used in this study, the effect of truncating the distributions at $D_m = 6$ mm and not carrying the integrations of the distribution to $D = \infty$ is negligible.

Now we explore the effects of truncation on the shape of the normalized distributions. Specifically, can truncating the distribution at $D = D_m$, instead of

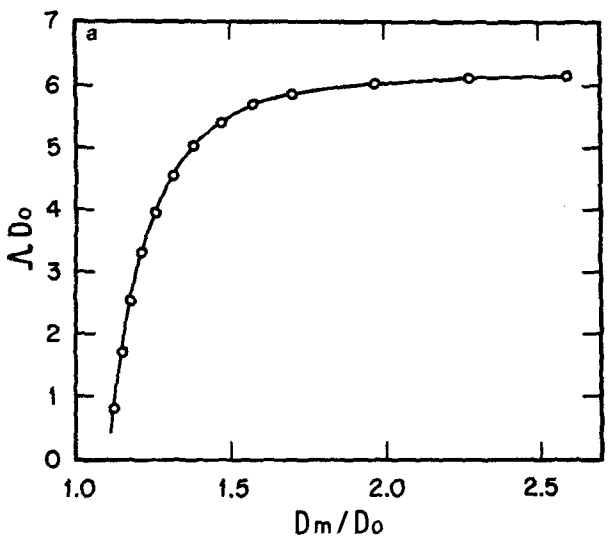

FIG. 4a. $D_0\Lambda(\beta)$ as a function of Dm/D_0 for a gamma distribution function (α = 2.5).

$D = \infty$, change an exponential distribution into one with curvature when normalized? An example M-P distribution for a rainfall rate of 50 mm h^{-1} and λ = 18.03 was normalized based on $D_m = \infty$ and then by using D_m = 0.31 cm. For this distribution, M_∞ = 2.378 g m^{-3} and $D_{0\infty}$ = 2.036 mm. For the truncated distribution, M = 1.933 gm^{-3} and D_0 = 1.787 mm. The distribution was then normalized using these truncated values. On a semilog plot, the normalized distribution is linear with an intercept of β^4/π and a slope of $-\beta$. For β = 3.67, this gives an intercept of 57.7 and a slope of −3.67. For the truncated distribution, the following adjustments apply:

$$\frac{\rho_w N(D) D_0^4}{M} = \frac{M_\infty}{M}\left(\frac{D_0}{D_{0,\infty}}\right)^4 \frac{\beta^4}{\pi} \times \exp\left[-\beta\left(\frac{D_0}{D_{0,\infty}}\right)\frac{D}{D_0}\right]. \quad (9)$$

This normalization of the truncated distribution gives a linear relation on a semilog plot with an intercept of 42.2 and a slope of −3.22. So the only effect of the rather extreme truncation at a D_m/D_0 = 1.75 is a lowering of the intercept and a flattening of the slope of the distribution. A distribution that is exponential does not have any curvature (on a semilog plot) added by the extreme truncation of the distribution at D_m = 0.31 cm. The instrument used in this study does not truncate the distribution until a diameter is nearly twice this value.

c. *Exponential and other gamma distribution function fits to the observed data*

Five functional fits to the observed data were selected for detailed examination and comparison. These five were selected because of either previous widespread application, or because of indications of improved goodness-of-fit. Three fits were exponential and were selected largely because of prior application; two were gamma distribution function fits, included largely because of the curvature indicated in the normalized distributions of Fig. 2. Ideally, one would like to have a functional fit grounded in the physics of drop formation, not only an empirical curve fit.

1) DESCRIPTION OF THE FITS

The first of the fits applied to the observed data was the classical Marshall–Palmer exponential distribution.

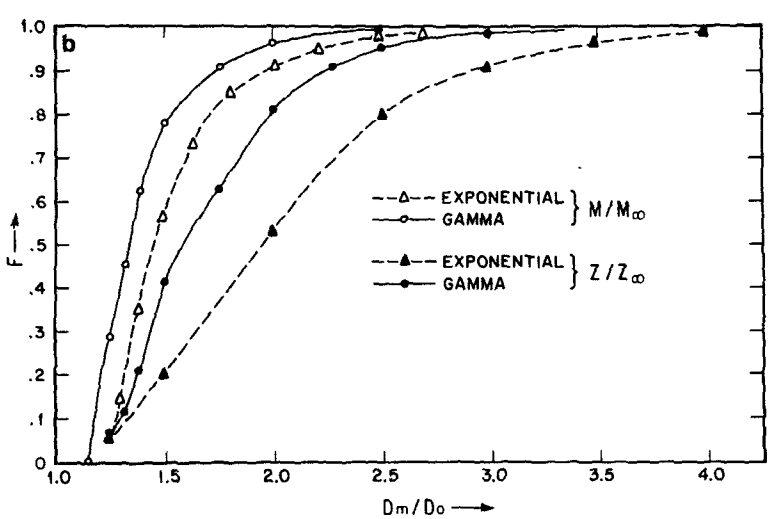

FIG. 4b. Z/Z_∞ and M/M_∞ as functions of Dm/D_0 for the exponential distribution (SS, 1970) and the gamma distribution function (α = 2.5).

This fit is based on Eqs. (1) and (2) with a fixed intercept parameter $N_0 = 0.08$.

The second fit was an "equivalent" or analytical exponential fit (AE), as outlined by Waldvogel (1974); N_0 and λ completely define an exponential fit to the drop size distribution. These parameters can be obtained by a simple transformation from two bulk parameters of the measured distribution. The two parameters used are the water content M and the radar reflectivity factor Z, both calculated by integrating the observed drop size distributions over the range of the instrument. The transformations are

$$N_0 = \frac{1}{\pi}\left(\frac{6!}{\pi}\right)^{4/3}\left(\frac{M}{Z}\right)^{4/3}(M), \tag{10}$$

$$\lambda = \left(\frac{6!}{\pi}\right)^{1/3}\left(\frac{M}{Z}\right)^{1/3}. \tag{11}$$

The third and final exponential functional fit was a linear least-squares fit to the logarithmic transformed data (LSE). This fit differs from the M–P exponential fit in that the intercept N_0 was not constrained. The squared error in $\log N(D)$ was minimized in the least-squares fit.

The final two fits involved the gamma distribution function. The first, termed "analytical gamma" (AG), is based on a fit to the normalized drop size distributions of Fig. 2. The normalization procedure is similar to that outlined in Section 3b. Using a simplified form of a gamma distribution comparable with (1),

$$N(D) = N_G D^{\alpha} \exp(-\Lambda D), \tag{12}$$

and the relation $D_0 = \beta/\Lambda$; then M_∞ is determined as in (4), i.e.,

$$M_\infty = \frac{\pi}{6}\frac{\rho_w N_G \Gamma(\alpha+4)}{\Lambda^{\alpha+4}} = \frac{\pi}{6}\frac{\rho_w N_G \Gamma(\alpha+4) D_0^{\alpha+4}}{\beta^{\alpha+4}}. \tag{13}$$

The normalized relation comparable with 6 is

$$\frac{N(D)\rho_w D_0^4}{M_\infty} = \frac{6}{\pi}\frac{\beta^{\alpha+4}}{\Gamma(\alpha+4)}\left(\frac{D}{D_0}\right)^{\alpha}\exp[-\beta(D/D_0)]. \tag{14}$$

The data of Fig. 2 were then input to a curvilinear least-squares routine to minimize the error squared about a function of the form of (12) and (14). This procedure resulted in

$$N_{\text{norm}}(D) = 492.7(D/D_0)^{2.56}\exp[-5.65(D/D_0)]. \tag{15}$$

This curvilinear least-squares fit to the normalized data with $\alpha = 2.5$ was used, along with the water content and median volume diameter calculated from the observed distribution, to determine a fit to each individual drop size distribution.

The second gamma distribution function fit and the final fitting scheme of the five used here, is an unconstrained three-parameter curvilinear least-squares fit (CG), minimizing the squared error in $\ln N(D)$. This routine was individually applied to each of the 112 measured drop size distributions.

The routine used is an iterative nonlinear least-squares grid search routine that minimizes the squared error about a function of the form of (12). The routine uses the LSE as a first-guess fit. The routine was adapted from Bevington (1969). The CG fits have a mean curvature parameter of about 2. The derived least-square relationships for the three fitted gamma distribution function parameters as a function of rainfall rate give, for $R = 50$ mm h^{-1}, $N_G = 36$, $\alpha = 1.9$ and $\Lambda = 32$.

2) Error criteria and performance of the fits

It is common practice to use a squared-error criterion as a measure of the goodness-of-fit. However, the goodness-of-fit may be more appropriately measured by the goodness of the estimate of coalescence growth and drop evaporation provided by the fit. This is, for some purposes, a more appropriate measure, since these are important microphysical processes that are required to be parameterized in numerical simulations. So, in addition to judging the goodness-of-fit based on squared error, we compared the estimates of coalescence growth and evaporation rate provided by each fit with those computed from the original observed distributions. These calculations were made using simple microphysical models.

The squared-error performance ($D > 300$ μm) of the five fits is shown in Table 1. The overall value and that for each of six class intervals of rainfall rate are shown. As would be expected, the fits that are based on minimizing squared error (LSE and CG) perform the best based on this criterion. The curvature of the gamma distribution (CG) does provide some improvement over the exponential, particularly at rainfall rates > 50 mm h^{-1}. Based on this unweighted error-squared criterion alone, one would choose either the least-squares exponential (LSE) or, for further refinement, the least-squares gamma (CG) fit.

d. Drop coalescence growth

We next examine how well these least-square criterion fits characterize drop coalescence, growth and drop evaporation. Parameterizations based on the classical Marshall–Palmer fit are in widespread use in numerical simulations. How well does this particular functional fit characterize coalescence growth and evaporation?

To assess the coalescence growth performance of the fits, a simple coalescence model was used. A monodisperse distribution of cloud droplets of radius

TABLE 1. Total squared error of log-transformed data.

	Data $[(N_{obs} - N_{fit})^2]$ ($cm^{-6} \times 2500$)				
R (mm h^{-1})	M-P	AE	LSE	AG	CG
200	9.55	12.12	7.07	8.65	5.72
150	7.40	14.40	6.27	8.44	5.67
100	19.59	33.71	17.05	16.45	12.38
75	49.28	62.97	35.34	43.80	33.67
50	16.32	21.27	12.40	14.02	11.13
25	30.20	31.04	20.34	22.73	17.71
10	51.86	27.20	17.29	29.57	22.02
0					
Total	184.19	202.71	115.77	143.65	108.30

TABLE 2a. Total coalescence growth squared error.

	M-P	AE	LSE	AG	CG
R (mm h^{-1})	(droplets s^{-1} cm^{-3})^2				
200	25.80	0.91	13.79	0.29	2.05
150	8.50	0.51	7.38	0.47	4.29
100	5.61	0.56	14.10	0.41	4.28
75	4.31	0.36	13.13	0.81	7.18
50	0.41	0.07	2.80	0.11	0.72
25	0.20	0.02	1.30	0.09	0.59
10	0.16	0.00	0.13	0.02	0.06
0					
Total	44.99	2.42	52.63	2.20	19.17

$r = 10$ μm and a concentration of 238.7 cm^{-3} was assumed. This gives a typical cloud liquid water content of 1 g m^{-3}. If collection efficiency E is defined as the radius of the swept cylinder (R), squared, divided by the radius of the large accreting drop (r_L), squared,

$$E = \frac{R^2}{r_L^2}, \tag{16}$$

then the rate of collection of cloud droplets is

$$\frac{dn_s}{dt} = r_L^2 E n_s (v_L - v_s), \tag{17}$$

where n_s is the concentration of small drops and ($v_L - v_s$) is the relative velocity between the collector and the collected drops. The collection efficiencies used for precipitation-sized drops collecting $r = 10$ μm drops were those tabulated by Young (1975), but the exact values are not critical to the results of these comparisons.

For each observed distribution, and each of the five fits to each observed distribution, the total coalescence growth was calculated. In each case, the coalescence growth error was calculated as the difference between the coalescence growth calculated ($D > 300$ μm) for the observed distribution minus that calculated for the particular fit. The resulting squared errors and average percent coalescence growth error are presented in Table 2.

These results are surprising in several respects. First, the two least-square criterion fits provide very poor estimates of coalescence growth. The exponential least-squares fit is very poor; in fact, it is worse than the classical Marshall–Palmer fit! From the standpoint of total squared error, the analytical gamma is slightly better than the analytical exponential, particularly at high rainfall rates. It is also surprising that the analytical exponential characterizes coalescence growth as well as it does, particularly since the goodness-of-fit under an error-squared criterion was so poor. Evidently, this scheme provides a reasonable measure of coalescence growth over the middle-sized drops, which are dominant in coalescence growth. Based on these results, both of the analytical schemes, exponential and gamma, are comparable and both are distinctly superior to the other three fits in characterizing coalescence growth.

A detailed example serves to illustrate the reason for these results. In Fig. 5, the fits to an example distribution and the corresponding coalescence growths are shown for each drop size interval. The exponential fits are shown in Fig. 5a. The M–P underestimates coalescence growth. The LSE underestimates the coalescence growth even more severely than the M-P. This underestimate is caused by the equal weight given to all drop sizes by the least-squares fitting routine. The fit at the very small and the very large drop diameters causes an underestimate of number concentrations through the size range responsible for the bulk of the coalescence growth. This results in a severe underestimation of total coalescence growth. The AE fit describes the total coalescence growth (area under the curve) very well, but the peak is near $D = 1$ mm instead of at the observed peak near $D = 2$ mm. The AE fit matches the total coalescence growth through compensating errors caused by too high a number concentration of drops at the smaller sizes and too low a concentration over the middle sizes. The two gamma distribution function fits are presented in Fig. 5b. The AG fit estimates the coalescence growth very well. The CG fit underestimates the coalescence growth at sizes of $D > 2$ mm. So, based on the examination of numerous such examples, as well as the overall result, it is concluded that the AG properly estimates the total

TABLE 2b. Average percent coalescence growth error.

R (mm h^{-1})	M-P	AE	LSE	AG	CG
200	26.95	5.25	19.88	2.48	6.36
150	16.38	4.26	15.83	4.07	10.05
100	10.66	4.51	21.02	3.94	11.60
75	8.80	3.54	20.08	5.45	14.41
50	9.02	3.58	22.66	4.60	12.51
25	11.05	2.87	27.10	7.69	16.69
10	39.34	1.61	19.72	8.58	15.03
0					
Average	16.32	3.41	21.09	5.72	13.43

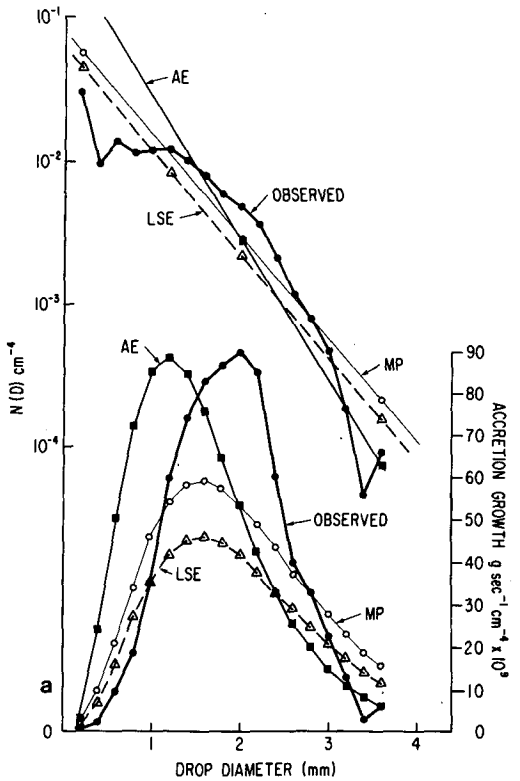

FIG. 5a. Example observed (upper) drop size distribution and exponential fits and (lower) associated calculated coalescence growth rates.

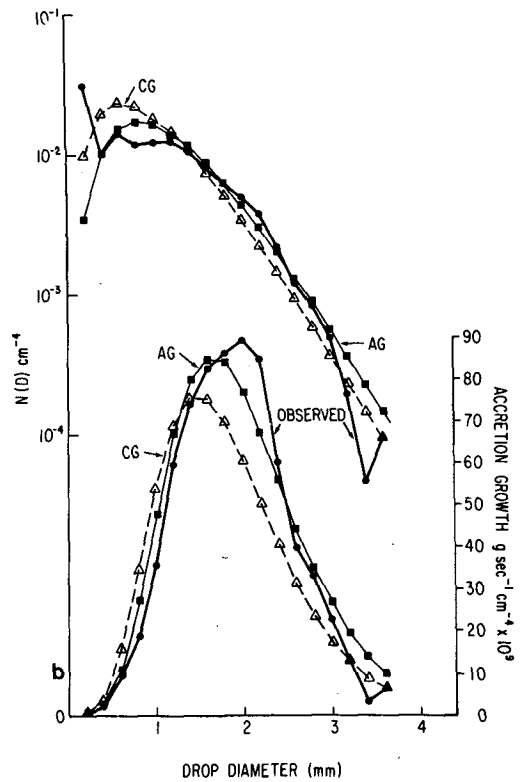

FIG. 5b. Example observed (upper) drop size distribution and gamma fits and (lower) associated calculated coalescence growth rates.

coalescence growth and matches the observed contributions of the individual drop size intervals as well. Of course, all that is really required of a parameterization is that it correctly estimate the total coalescence growth. The AE is comparable with the AG in this regard, but, as seen in the next section, has serious shortcomings in describing drop evaporation.

e. Drop evaporation

As in the case of coalescence growth, a simplified model of drop evaporation was applied to assess the performance of the five fits in characterizing drop evaporation. When the evaporation of freely falling drops is described, the convective enhancement of the evaporation rate is paramount. The mean ventilation coefficient f_v is defined as the ratio of the water mass from a moving drop (dm/dt) to that of a motionless drop [$(dm/dt)_0$]:

$$f_v = \frac{dm/dt}{(dm/dt)_0}. \tag{18}$$

The steady-state rate of change of mass for a motionless drop of radius a is

$$(dm/dt)_0 = 4\pi a D_v(\rho_{v,\infty} - \rho_{v,a}), \tag{19}$$

where D_v is the diffusivity of water vapor in air, $\rho_{v,\infty}$ the environmental vapor density and $\rho_{v,a}$ the vapor density at the drop surface. An alternative expression in terms of vapor pressure e and temperature T is found by substituting the equation of state, i.e.,

$$\frac{dm}{dt} = 4\pi a D_v \frac{M_w}{R}\left(\frac{e_\infty}{T_\infty} - \frac{e_a}{T_a}\right), \tag{20}$$

where R is the universal gas constant and M_w the molecular weight of water.

Kinzer and Gunn (hereafter, KG) (1951) experimentally determined the evaporation rate of freely falling drops. Their results reportedly were plagued by inaccuracies in the experimental setup and the assumed or determined values for the vapor diffusivity, drop surface temperature and terminal velocities. Pruppacher and Rasmussen (hereafter, PR) (1979) and Beard and Pruppacher (1971) have more recently experimentally determined the evaporation rate of freely falling drops. They find that the following relation applies for drops from $D = 120$ μm to $D = 5$ mm:

$$f_v = 0.78 + 0.308X, \tag{21}$$

where $X = N_{Sc}^{1/3} N_{Re}^{1/2}$, N_{Re} is the Reynolds number and N_{Sc} is the Schmidt number, which is defined as N_{Sc}

TABLE 3a. Total drop evaporation squared error.

R (mm h^{-1})	M-P	AE	LSE	AG	CG
			$(g\ s^{-1})^2$		
200	3.203	4.939	0.622	0.061	0.387
150	0.915	3.221	0.334	0.036	0.631
100	0.499	4.530	0.892	0.064	0.412
75	1.054	3.614	0.921	0.089	0.735
50	0.117	0.989	0.197	0.038	0.070
25	0.165	0.379	0.144	0.025	0.070
10	0.152	0.043	0.024	0.007	0.014
0					
Total	6.103	17.710	3.135	0.321	2.320

$= \mu/\rho D_v$, where μ is the dynamic viscosity of air and ρ the air density.

The evaporation calculations were performed using both the results of KG and the more recent experimental results of PR. Both evaporation formulations gave the same qualitative results, so only the results from the more recent PR (1979) formulation of evaporation are reported here. The total rate of evaporation was calculated for each observed size distribution ($D > 300$ μm) and, in addition, for each of the five fits to each observed distribution. The assumed environmental conditions were surface pressure, $T = 20$°C and 70% relative humidity.

The error-squared and average percent drop evaporation error results are presented in Table 3. Of particular significance here is that the AE fit, which did well in characterizing coalescence growth, is a very poor estimator of drop evaporation. The AG fit estimates drop evaporation very well. The two least-square-criterion fits are better estimators of drop evaporation than they were estimators of coalescence growth. The M-P is a poor estimator of evaporation at low rainfall rates. This analysis shows that the analytical gamma distribution has considerable potential for parameterizing drop evaporation, as well as coalescence growth.

Details of the evaporation calculation for the example distribution of Fig. 5 are presented in Fig. 6. This example clearly indicates that the small drop region is the problem area for the analytical exponential fit. The evaporation rates calculated from the analytical

TABLE 3b. Average percent drop evaporation error.

R (mm h^{-1})	M-P	AE	LSE	AG	CG
200	27.10	35.31	11.68	3.48	9.24
150	13.44	32.39	9.32	2.83	13.05
100	9.52	36.50	14.23	3.63	10.49
75	13.49	30.88	14.85	4.69	13.54
50	12.82	35.56	15.46	6.25	8.56
25	26.55	35.57	21.33	8.60	13.55
10	88.64	27.82	16.81	9.71	13.37
0					
Average	28.43	32.74	15.47	5.90	12.32

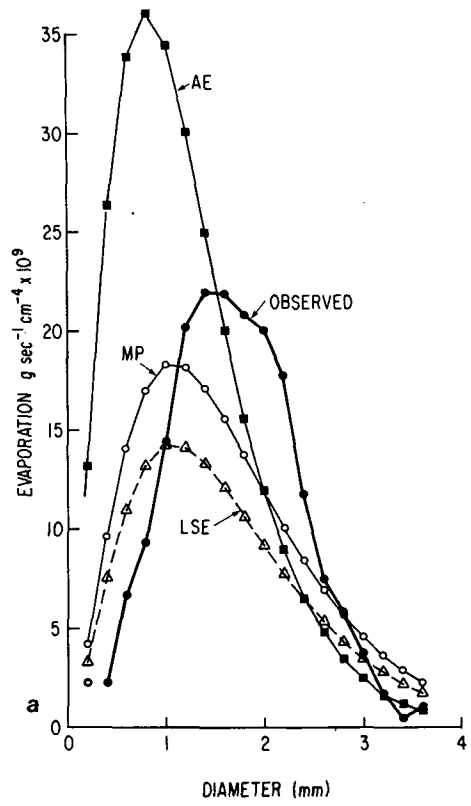

FIG. 6a. Calculated drop evaporation rate for observed distribution and exponential fits of Fig. 5.

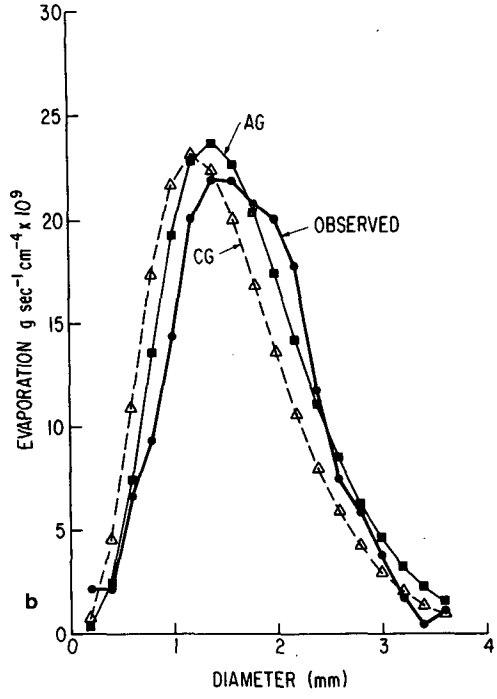

FIG. 6b. Calculated drop evaporation rate for observed distribution and gamma fits of Fig. 5.

gamma fit agree quite well with those calculated from the observed drop number densities over the entire size range. Although it is not clear from this particular example, the CG fit tended to overestimate drop evaporation. Thus for drop evaporation, as was the case for coalescence, the fits which are best from a squared-error standpoint do not provide the best measures of drop evaporation. The results are based on simplified models, but these models do capture the essence of the physical processes involved.

f. Applicability of results

Although these data were measured in tropical convective systems, the basic physics controlling the shape of the drop spectrum should be essentially the same in any high-water-content cloud with substantial depth of warm cloud below the level of ice involvement. Above some threshold of precipitation water content in the warm cloud, the evolution of the drop distribution is controlled by a balance between raindrop growth, due to collision coalescence and accretion of cloud droplets, and contraction of raindrop size, due to collision breakup. This balance appears to result in a larger relative decrease in the number concentrations at the large drop end of the spectrum than at the small- to middle-sized ranges.

The following evidence is presented to support the hypothesis that the balance between coalescence growth and collision breakup shapes the drop spectrum regardless of geographical location or the details of the microphysical processes that initiated the precipitation. First, Atlas (1964) examined Z–R data points from a wide range of conditions and geographic areas on a rain parameter diagram. He found that all of the Z–R lines converge at rainfall rates between 20 and 50 mm h^{-1}. He concludes that this indicates that all such heavy rains are essentially identical in character (and perhaps origin as well), regardless of climate.

Next, a set of drop size distributions from a continental location has the same shape. A sample of fairly high rain rate distributions (Mueller and Sims, 1967) measured with a drop camera at Franklin, North Carolina (35.03°N, 83.47°W) during July and August, were normalized identically to the data of Fig. 2. The results of this normalization are presented in Fig. 7. Although the curvature is not as immediately obvious as in Fig. 2, the objective fit to the data points is

$$N_N(D) = 535.9 D_N^{2.52} \exp(-5.71 D/D_0), \quad (22)$$

which is very close to the objective fit to the data of Fig. 2 [Eq. (15)]. In this data sample, drops < 0.5 mm diameter were not measured, but even so there is considerable scatter at the small-sized end of the spectrum. The low-concentration points are probably due to the effects of evaporation below cloud base, but the few high-concentration points are puzzling. The high scatter notwithstanding, the objective fit to these data from

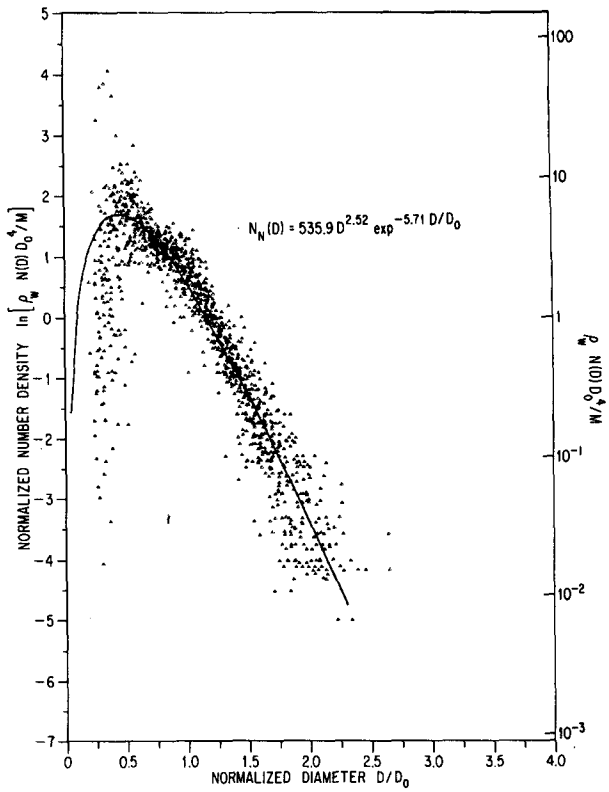

FIG. 7. Normalized drop size distributions, July–August, Franklin, North Carolina.

a continental location is the same as the oceanic–tropical sample.

Datasets analyzed by Takeuchi (1978) indicate the correctness of the gamma fit, but he found a larger curvature parameter. His data included low-slope distributions very similar to those of Carbone and Nelson (hereafter, CN) (1978). Even so, a plot of the entire dataset normalized the same as Fig. 2 has a shape similar to that of Fig. 2. As discussed earlier, the curvature in the instantaneous shapes of Joss and Gori (1978) are similar to the results of this study, although their high rate distributions are characterized by the occurrence of larger drops.

The data of this study are in disagreement with the original data of M–P for the reasons that their data: 1) covered only $D > 1$ mm, 2) were averages over many distributions, which would tend to mask any curvature, and 3) were not from predominantly warm-based convective clouds. Data at variance with the data of this study, which are from warm-based convective clouds and should be mentioned here, have been presented by CN. Their distributions contain very much lower concentrations of small drops and much higher concentrations of large drops than either the distributions of this study or the M–P distributions. They attribute this disparity to the effects of sedimen-

tation, although it is difficult to see how this transient phenomenon could pervade an entire dataset.

Some disagreement notwithstanding, based on the data of this study, a gamma distribution function with a constant curvature parameter of 2.5 is proposed to characterize the drop size distributions from convective clouds. This fit models the observed distributions particularly well over the size ranges important in coalescence growth and provides a good estimate of drop evaporation.

4. Proposed modifications to Marshall–Palmer fits in cloud microphysical parameterization schemes

The Marshall–Palmer distribution has been widely applied in parameterizations of cloud microphysical processes for numerical simulations of cloud-scale and larger scale processes (Kessler, 1969). In this section, changes to the M–P based parameterizations of rainwater are proposed based on the analytical gamma fit. These changes should result in improved parameterizations of coalescence growth and evaporation.

The changes proposed here involve only the distribution of precipitation (rain) water after its initial formation (by autoconversion, or its alternative). We propose to distribute the precipitation water according to a gamma distribution function with a curvature parameter of $\alpha = 2.5$, based on the observed sample of normalized distributions. Once the initial conversion to precipitation water occurs, i.e., when M is determined, it is proposed to distribute this water as follows:

1) The median volume diameter is computed from the empirically derived relation (see the Appendix)

$$D_0 = 0.157M^{0.168}, \tag{23}$$

where M is in g m^{-3} and D_0 is in cm.

2) Next, M is distributed into a drop size distribution based on the fit to the normalized data using the following,

$$N(D) = N_G D^{\alpha} \exp(-\Lambda D), \tag{24}$$

$$N_G = \frac{6.36 \times 10^{-4} M}{D_0^4}\left(\frac{1}{D_0}\right)^{2.50}, \tag{25}$$

$$\alpha = 2.50$$

$$\Lambda = 5.57/D_0, \tag{26}$$

where $N(D)$ is in cm^{-4}, M is in g m^{-3} and D_0 is in cm.

The resultant fit to an example spectrum where $M = 2.584$ g m^{-3} is plotted in Fig. 8.

Once the drop size distribution is defined, the fallspeed of the median volume drop size, the rainfall rate, the coalescence growth of raindrops and drop evaporation can be found by appropriate numerical integrations.

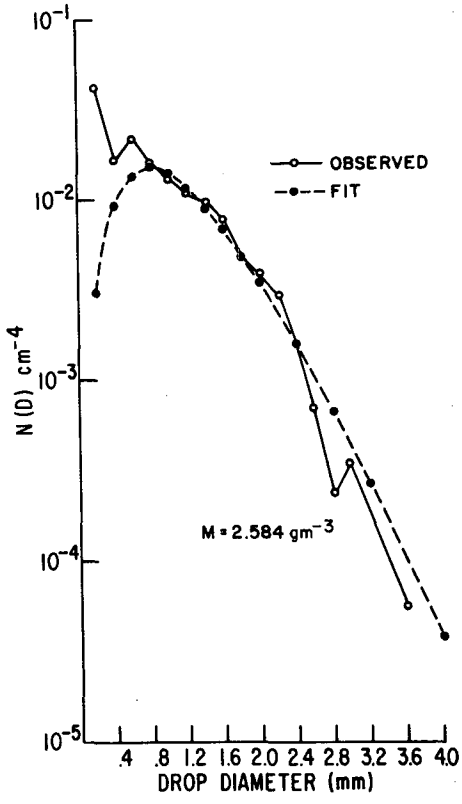

FIG. 8. Example observed distribution and functional fit.

Alternatively, analytical expressions can be used. The following analytical expressions were derived based on the analytical gamma distribution, but otherwise using Kessler's (1969) approximations and curve fits:

- ACCRETION GROWTH

$$\frac{dM}{dt}(\text{g m}^{-3}\text{ s}^{-1}) = 1.2252 \times 10^5 \frac{N_G \bar{E} m}{\Lambda^6}, \tag{27}$$

where $\bar{E}$ is the number density weighted mean collection efficiency and m is the cloud water content in g m^{-3}.

- EVAPORATION

$$\frac{dM}{dt}(\text{g m}^{-3}\text{ s}^{-1}) = \frac{3.9476 \times 10^2 m N_G}{\Lambda^{5.1}}, \tag{28}$$

where m is now the negative cloud water or saturation deficit.

- VELOCITY OF MEDIAN VOLUME DROP

$$V_0 = 7.543 \times 10^2 N_G^{-1/13} M^{1/13}. \tag{29}$$

The above analytical expressions were derived with the terminal velocity expression $V_T = 1300D^{1/2}$ (Kessler, 1969). Uplinger (1981) has fitted Kinzer and Gunn's terminal velocity data with the following function and found <2% error over the normal full range of raindrop sizes:

$$V_T = 4854D \exp(-1.95D). \tag{30}$$

When we use this expression for terminal velocity, the expression for coalescence growth becomes

$$\frac{dM}{dt} = \frac{1.0975 \times 10^6 \bar{E} N_G m}{(\Lambda + 1.95)^{6.5}}. \tag{31}$$

The improvement in the parameterization of coalescence growth and drop evaporation, as indicated by Tables 2 and 3, is worth the slight extra complication of using a three-parameter distribution. Only minor changes are required to the presently used Marshall–Palmer-based parameterizations. Further testing will be required, but it is clear that the proposed functional fit is superior to the exponential fits in the size ranges important in coalescence growth. It provides a reasonable characterization of drop evaporation, as well. Miller and Pearce (1974) found that the details of the cloud dynamics in a three-dimensional model are quite sensitive to assumptions made regarding the cloud microphysics. They noted that significant rapid changes which occurred at times in the model cloud's history were governed primarily by the details of the assumed cloud microphysical processes.

5. Summary and conclusions

This study presents the results of an analysis of a sample containing 112 drop size distributions. Each distribution was measured over approximately 1.3 km of flight track with an airborne optical spectrometer. The data sample is from predominantly convective clouds in two hurricanes and covers a wide range of rainfall rates. After normalization, a plot of all the drop size distributions, now independent of rainfall rate, indicates a departure from a purely exponential size distribution. Numerous investigators have concluded that the Marshall–Palmer distribution function, while fitting overall average distributions, does not realistically describe individual measurements at both the smaller and larger size ranges. The present analysis supports that conclusion; fewer small drops and slightly fewer large drops are found in comparison with the M–P distribution.

Three exponential fits and two gamma distribution function fits were applied to the data and compared. It was found that unweighted least-squares fits, although they provided the best fits based on squared error alone, did very poorly in characterizing coalescence growth and did not give the best estimates of drop evaporation. An analytical gamma distribution function fit to the measured distributions provided the best compromise between satisfactory error-squared fit and realistic characterization of coalescence growth and drop evaporation. Relations between parameters of the distributions were derived and are summarized and compared in the Appendix.

Based on the improved characterization of coalescence growth and evaporation by the analytical gamma fit, modifications to the Marshall–Palmer based microphysics parameterizations are proposed. Precipitation water, after its initial conversion from cloud water, is proposed to be distributed according to a gamma distribution function (12), the parameters of which are based on a fit to the normalized data sample. The method consists of finding the median volume diameter D_0 from an empirical D_0—M relationship and then letting $\alpha = 2.5$; N_G and Λ are calculated from the fit to the normalized data. Alternate expressions to the M–P based relationships for coalescence growth, drop evaporation and terminal velocity of the median volume diameter drop are derived based on the gamma distribution function fit. The improvement in the estimates of coalescence growth based on the results of Section 3 indicate that the extra complication of a three-parameter distribution is worthwhile.

Although the drop distributions analyzed here are from hurricane clouds, the basic physical processes shaping the drop spectra are probably the same as for any warm-based convective cloud. Therefore, these results should apply to any convective cloud system with a significant depth of warm rain processes. Exploration of stratifications of the data by altitude and vertical wind velocity and further comparisons of data from oceanic and continental convective clouds are planned in subsequent work.

Acknowledgments. The engineers, technicians and flight crews of the Office of Aircraft Operations deserve thanks for their skilled efforts in data collection. Mr. David Jorgensen deserves credit for his concerted effort on the data reduction software. Thanks are due to Dr. Stephen Lord and Mr. David Jorgensen for their helpful suggestions. Connie Arnhols, Dale Martin, Angel Tillman and Marie Willis deserve credit and thanks for editorial reviews, figure drafting and typing of the manuscript.

APPENDIX

Equations Relating Parameters of the Distributions

In this appendix, relationships between measured parameters of the distributions are derived. These are linear least-squares lines of best fit between the parameter pairs. The derived relations are summarized and compared in Table A1.

TABLE A1. Summary of derived relations and comparisons.

Parameter	Relation	M-P (1948)	SS (1971)
M-R	$M = 0.062\ R^{0.913}$	$M = 0.072\ R^{0.88}$	$M = 0.052\ R^{0.94}$
Z-R	$Z = 276.7\ R^{1.290}$	$Z = 200\ R^{1.6}$	$Z = 300\ R^{1.35}$
D_0-R	$D_0 = 0.097\ R^{0.158}$	$D_0 = 0.09\ R^{0.21}$	$D_0 = 0.13R^{0.14}$
D_0-M	$D_0 = 1.571\ M^{0.1681}$	—	—
Λ-R	$\Lambda = 37.15\ R^{-0.125}$	$\Lambda = 41\ R^{-0.21}$	$\Lambda = 38\ R^{-0.14}$
N_0-R	$N_0 = 0.038R^{+0.412}$	$N_0 = 0.08$	$N_0 = 0.07\ R^{0.37}$
Λ-M	$\Lambda = 25.3023\ M^{-0.132}$	$\Lambda = 21.9\ M^{-0.239}$	$\Lambda = 25\ M^{-0.15}$
N_0-M	$N_0 = 0.13041\ M^{0.472}$	$N_0 = 0.08$	$N_0 = 0.23\ M^{0.40}$

REFERENCES

Atlas, D., 1953: Optical extinction by rainfall. *J. Meteor.*, **10,** 486–488.

——, 1964: Advances in radar meteorology. *Advances in Geophysics,* Vol. 10, H. E. Landsberg and J. Van Mieghem, Eds., Academic Press, 318–484.

Beard, K. V., and H. R. Pruppacher, 1971: A wind tunnel investigation of the rate of evaporation of small water drops falling at terminal velocity in air. *J. Atmos. Sci.*, **28,** 1455–1464.

Bevington, P. R., 1969: *Data Reduction and Error Analysis for the Physical Sciences.* McGraw Hill, 336 pp.

Brown, P. S., 1981: Time constant variation in the collision breakup equation. *J. Atmos. Sci.*, **38,** 2758–2762.

Carbone, R. E., and L. D. Nelson, 1978: The evolution of raindrop spectra in warm-based convective storms as observed and numerically modeled. *J. Atmos. Sci.*, **35,** 2302–2314.

Jorgensen, D. P., and P. T. Willis, 1982: A Z-R relationship for hurricanes. *J. Appl. Meteor.*, **21,** 356–366.

Joss, J., and E. G. Gori, 1978: Shapes of raindrop size distributions. *J. Appl. Meteor.*, **17,** 1054–1061.

Kessler, E., 1969: *On the Distribution and Continuity of Water Substance in Atmospheric Circulations. Meteor. Monogr.,* No. 32, Amer. Meteor. Soc., 48 pp.

Kinzer, G. D., and R. Gunn, 1951: Evaporation of freely falling raindrops. *J. Meteor.*, **8,** 71–83.

Knollenberg, R. G., 1981: Techniques for probing cloud microstructure. *Clouds, Their Formation, Optical Properties and Effects,* P. V. Hobbs and A. Deepak, Eds., Academic Press, 15–92.

List, R., and J. R. Gillespie, 1976: Evolution of raindrop spectra with collision induced breakup. *J. Atmos. Sci.*, **33,** 2007–2013.

Marshall, J. S., and W. M. Palmer, 1948: The distribution of raindrops with size. *J. Meteor.*, **5,** 165–166.

Miller, M. J., and R. P. Pearce, 1974: A three-dimensional primitive equation model of cumulonimbus convection. *Quart. J. Roy. Meteor. Soc.*, **100,** 133–154.

Mueller, E. A., and A. L. Sims, 1966: Radar cross sections from drop size spectra. Tech. Rep. ECOM-00032-F, Contract DA-28-043 AMC-00032(E) Illinois State Water Survey, Urbana, 110 pp. [AD-645218].

——, and ——, 1967: Raindrop distributions at Franklin, North Carolina. Tech. Rep. ECOM-02071-RR3, Contract DA-28-043 AMC-02071(E) Illinois State Water Survey, Urbana, 157 pp. [AD-822042].

Pruppacher, H. R., and R. Rasmussen, 1979: A wind tunnel investigation of the rate of evaporation of large water drops falling at terminal velocity in air. *J. Atmos. Sci.*, **36,** 1255–1260.

Rogers, R. R., 1979: *A Short Course in Cloud Physics,* 2nd ed. Pergamon Press, 235 pp.

Sekhon, R. S., and R. C. Srivastava, 1970: Snow size spectra and radar reflectivity. *J. Atmos. Sci.*, **27,** 299–307.

——, and ——, 1971: Doppler observations of drop size distributions in a thunderstorm. *J. Atmos. Sci.*, **28,** 983–994.

Srivastava, R. C., 1971: Size distribution of raindrops generated by their breakup and coalescence. *J. Atmos. Sci.*, **28,** 410–415.

——, 1978: Parameterization of raindrop size distributions. *J. Atmos. Sci.*, **35,** 108–117.

Takeuchi, D. M., 1978: Characterization of raindrop size distributions. *Preprints Conf. Cloud Physics and Atmospheric Electricity,* Issaquah, Amer. Meteor. Soc., 154–161.

Ulbrich, C. W., 1981: Effect of size distribution variations on precipitation parameters determined by dual-measurement techniques. *Preprints 20th Conf. Radar Meteorology,* Boston, Amer. Meteor. Soc., 276–281.

Uplinger, W. G., 1981: A new formula for raindrop terminal velocity. Proc., *20th Conf. Radar Meteorology,* Boston, Amer. Meteor. Soc., 389–391.

Waldvogel, A., 1974: The N_0 jump of raindrop spectra. *J. Atmos. Sci.*, **31,** 1067–1078.

Young, K. C., 1975: The evolution of drop spectra due to condensation, coalescence and breakup. *J. Atmos. Sci.*, **32,** 965–973.